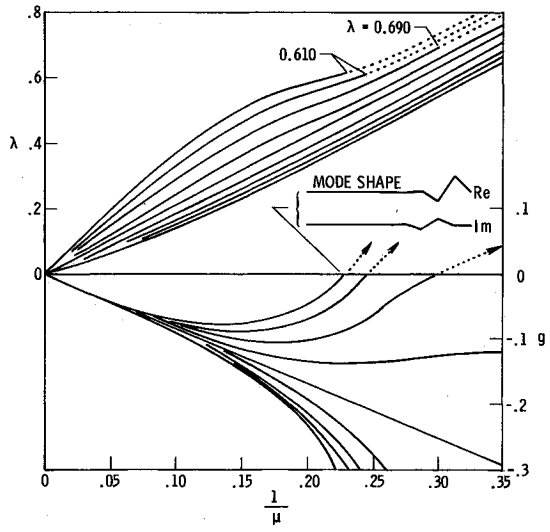

Fig. 2 Plots of dynamic pressure parameter λ and associated structural damping coefficient g vs mass ratio $1/\mu$, for $M = 2.0$, $B = 10$, and $k_s = 0.6$.

at an indicated point of neutral flutter stability are also shown. The segment juncture closest to the trailing edge has the largest amplitude, while the forward 60% has very small amplitude. This flutter mode shape is typical of the present analytical results.

The use of other Mach numbers verifies that combinations of $1/\mu$ and M that give the same ratio $1/\mu M$ give identical results. Figure 3 gives flutter boundaries plotted against $1/\mu M$ that are essentially coincident for $B = 4$, 10, and 20. These boundaries are, of course, the loci of the neutral stability points for $g = 0$ with the lowest λ for a range of $k_s = 0.0$ to about 1.0. The point from Fig. 2 is labeled. The flutter boundary slopes upward to the right because of the aerodynamic-damping term in the piston theory. The result of using only the static slope term in the downwash of Eq. (9) is shown by the horizontal boundary labeled "static aerodynamics only."

The small crosshatched region in the lower left of Fig. 3 covers the region of expected maximum dynamic pressure during launch, using the $\bar{k}$ and m_s of a candidate design being studied.

Conclusions

The panel flutter characteristics of a candidate thermal protection system (TPS) for the space shuttle have been analyzed based on piston theory aerodynamics and Lagrange's equations. The panel was analyzed as being simply supported at leading and trailing edges and made up of a number of uniform rigid segments hinged together and supported on springs at the segment junctures. For zero structural damping, a single flutter boundary of dynamic pressure parameter vs a mass ratio parameter was found to apply for all Mach numbers to which piston theory is applicable. A variation in the number of panel segments from 4 to 20 was found to have practically no effect on the flutter boundary. Use of the parameters of a conceptual design being studied for the TPS along with the maximum launch dynamic pressure and the associated Mach number predicts the TPS candidate panel array to be deep in the "no-flutter" region during launch and, therefore, safe from panel flutter.

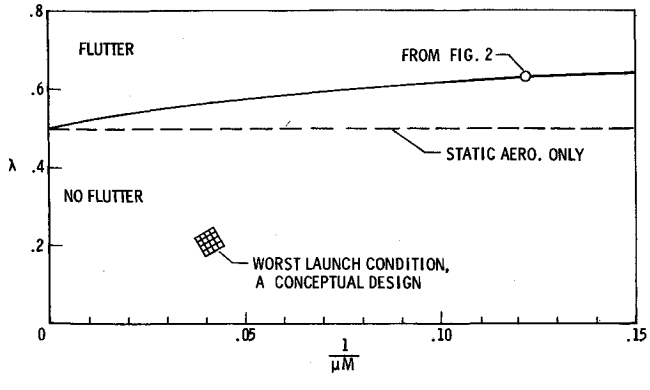

Fig. 3 Flutter boundary of λ vs $1/\mu M$ for $B = 4$, 10, and 20 with and without the aerodynamic damping of piston theory.

Application of Rice's Exceedance Statistics to Atmospheric Turbulence

WEN-YUAN CHEN*
NASA Langley Research Center, Hampton, Va.

Introduction

THE exceedance statistics of atmospheric turbulence have a direct bearing on the analysis of dynamic response of aircraft structures. The basic concepts of the theory of exceedance statistics are due to Rice.[1] He has derived a simple, yet important equation for the prediction of expected number of times per second, $N(\alpha)$, that the random disturbance will cross the value α. In order to apply his equation, the random fluctuation ought to be a stationary Gaussian process. In the literature, the velocities in individual patches of turbulence encountered by aircraft under different atmospheric conditions have been reported as stationary and Gaussian[2-4] to a sufficient extent to permit many practical applications. The estimation of exceedance statistics by Rice's equation was considered one of such.

Recent evidence,[5] however, indicates that there is disagreement between the measured exceedance values and the theoretical predictions given by Rice's equation. In an unpublished paper, R. Steiner, Langley Research Center, has suggested that the discrepancy may be due to the effect of multiple inputs to the airframe or due to the nonlinear response of the aircraft. In Ref. 5, it was suggested that nonstationary time trends in the data sample may cause the discrepancy. The purpose of the present work is to offer another explanation and to present some experimental evidence to support it.

Atmospheric turbulence is in general not a stationary nor a normal process. However, for a particular patch of turbulence or a segment of the patch, it might be fairly stationary both in the mean and in the variance. For such turbulence, the first-order distribution will usually appear to have a rather good Gaussian form. Yet, its second-order distribution will invariably turn out to be non-Gaussian, as will be evident later, indicating strongly that the turbulence is not a Gaussian process. It is emphasized that Rice's equation is built on the premise that the second-order distribution of a random process is joint-normal. It is then obvious that the application of Rice's exceedance statistics to atmospheric turbulence is bound to produce a discrepancy, regardless of the fact that the process is stationary and its first-order distribution is normal.

Theoretical Considerations

In order to stress the point that good Gaussian appearance of the first-order distribution alone is not adequate to insure a successful application of Rice's formula, let us study carefully the fundamental assumptions behind it. We shall adopt the route developed by Papoulis[6] to arrive at Rice's simple result in order to examine the assumptions involved. By adopting Papoulis'

Presented as Paper 72-136 at the AIAA 10th Aerospace Sciences Meeting, San Diego, Calif., January 17–19, 1972; submitted January 3, 1972; revision received March 28, 1972.

Index category: Aircraft Gust Loading and Wind Shear.

* NRC-NASA Resident Research Associate.

route, we may avoid the necessity of the experimental observation of the joint distribution of velocities and accelerations of air motion at the same instants, which is not presently available.

Let $X(t)$ be a zero-mean time history from which turbulence data samples were obtained. Consider two time instants t and $t + \tau$, and let $X_1 = X(t)$ and $X_2 = X(t + \tau)$. The probability that $X(t)$ crosses zero an odd number of times in the interval of $(t, t + \tau)$, denoted by $n_\tau(0)$, is equal to the probability that X_1X_2 is negative; that is,

$$n_\tau(0) = P\{X_1X_2 < 0\} = 2\int_0^\infty \int_{-\infty}^0 f(x_1,x_2)dx_1dx_2 \qquad (1)$$

In order to integrate Eq. (1), the exact form of $f(x_1,x_2)$ should be given. Let us first assume it is joint-Gaussian, but keep in mind that the assumption should be subjected to experimental confirmation later on. The integration would then yield

$$\cos[\pi n_\tau(0)] = \rho = R(\tau)/R(0) \qquad (2)$$

where ρ and $R(\tau)$ are correlation coefficient and correlation function of $X(t)$, respectively. For small τ, the probability of more than one zero-crossing is negligible, and therefore, with $n(0)$ denoting the probability that $X(t)$ crosses zero only once in the interval τ, $n(0)$ will be approximately equal to $n_\tau(0)$. In addition, with small τ, Eq. (2) can be greatly simplified to

$$n(0) = (1/\pi)[-R''(0)/R(0)]^{1/2}\tau \qquad (3)$$

indicating that $\ln(0)$ is linearly proportional to τ for small τ. The constant of proportionality, denoted by $N(0)$, is Rice's expected number of zero-crossings per unit time:

$$N(0) = (1/\pi)[-R''(0)/R(0)]^{1/2} \qquad (4)$$

For crossings of an arbitrary level, if X_1 and X_2 are jointly Gaussian and τ is small so that ρ is close to 1, it can be shown that

$$N(\alpha) = N(0)\exp(-\alpha^2/2\sigma^2) \qquad (5)$$

where σ^2 is the variance of $X(t)$. Eq. (5) states that $\ln N(\alpha)$ is proportional to α^2 with slope $-(2\sigma^2)^{-1}$. As mentioned previously, the predictions of Eq. (5) have been found to deviate substantially from experimental measurements.

Here we emphasize that a joint Gaussian distribution of $f(x_1,x_2)$ has been assumed in order to integrate Eq. (1) and, of equal importance, only small τ has been considered in order to arrive at the simple relation of Eq. (4). Both assumptions have been applied once more in order to achieve the goal of Eq. (5). The degree to which these two conditions are met, therefore, appears to be most important in understanding what causes the discrepancy mentioned above. Let us proceed to examine the experimental results.

Experimental Observations

The data sources are: a) High Altitude Clear Air Turbulence[5] (HICAT), b) Severe Storm Turbulence[4] (SEST), c) Barbados Oceanographic and Meteorological Experiment[7] (BOMEX), and d) Wind Tunnel Turbulence[8] (WITT). In most cases of HICAT and SEST, the data records have wide variations in variance over the record length. The nonstationary variance will affect severely the results of probability distributions, as reported by Crooks et al.[5] In view of this fact, particular care has been directed to the selection of segments of turbulence that have fairly stationary variance over the entire segment so that nonstationary effects may be neglected. Such selected segments usually consist of only a small number of data samples. BOMEX and WITT data, on the other hand, provide very long data records that are stationary both in the mean and the variance. For those presented in Figs. 1 and 2, the stationary segments for HICAT and SEST have data samples ranging only from 1024 to 2048, compared with 409,600 samples used for each run of BOMEX and WITT. The enormous difference in number of data samples is partly due to the different sampling rates used, which are 12.5 samples/sec for HICAT, 20 for SEST, 521 for BOMEX, and 16,000 for WITT.

In these empirical studies, we have followed the common practice of assuming that the process is ergodic and have performed all averages temporally. Fig. 1 shows the normalized first-order probability functions for all four measurements. Gaussian densities are also shown in the same figure. The experimental results are fairly normal when compared with the corresponding Gaussian curve. Standard deviation σ and kurtosis coefficient K, defined as the fourth moment of the zero-mean random variable divided by the square of the second moment, are listed for each run. The kurtosis coefficient can be interpreted as a measure of the departure from a Gaussian distribution, as it would be 3 for a Gaussian distribution. The measured K values show a little scattering about 3, but they are, nevertheless, very close to 3 for all four cases.

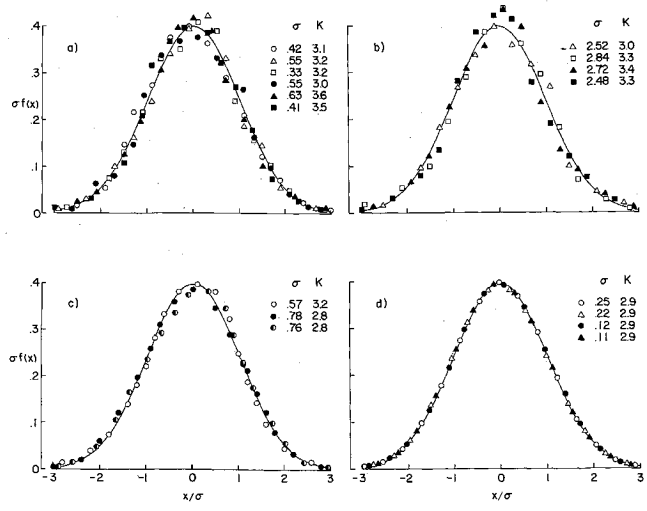

Fig. 1 Normalized probability density functions of X compared with Gaussian law: a) HICAT; b) severe storm turbulence; c) BOMEX; d) wind-tunnel turbulence. Circles are for streamwise components; triangles for lateral; squares for vertical. Open symbols are for first run; closed for second run; semiclosed for third run. The unit of σ is m/sec.

The apparent normality of the distribution of $X(t)$ does not insure that the joint distribution of X_1 and X_2, separated by a small interval τ as required by second assumption, will be Gaussian. To see whether $f(x_1,x_2)$ is Gaussian or not, the most direct way is to evaluate $f(x_1,x_2)$ and compare the results with the joint Gaussian law. Since $f(x_1,x_2) = f(x_2|x_1)f(x_1), f(x_1,x_2)$ can be determined by obtaining the conditional probability of X_2 for a set of constant values of X_1. However, this kind of evaluation requires an enormous number of data samples to get a reliable statistical value. Most of the available atmospheric turbulence measurements do not meet this requirement. Fortunately, there is an alternative way. If $f(x_1,x_2)$ is joint-Gaussian, the random variable $Z = X_1 - X_2$ should be distributed normally, as can be verified easily from the following equations:

$$F(z) = P\{Z \leqq z\} = \int_{-\infty}^{\infty}\int_{-\infty}^{z+x_2} f(x_1,x_2)\,dx,dx_2 \qquad (6)$$

$$f(z) = \int_{-\infty}^{\infty} f(z + x_2, x_2)\,dx_2 \qquad (7)$$

Substituting joint-Gaussian law into Eq. (7) for integration yields

$$f(z) = [1/(2\pi)^{1/2}\sigma_z]\exp(-z^2/2\sigma_z^2) \qquad (8)$$

where $\sigma_z^2 = 2\sigma^2(1 - \rho)$. Eq. (8) indicates that Z should be distributed normally with variance σ_z^2. If the distribution of Z turns out to be non-Gaussian, it must be because $f(x_1,x_2)$ is not joint-Gaussian.

The experimental values of $f(z)$, obtained directly from the new random variable $Z(= X_1 - X_2)$, are shown in Fig. 2, again in normalized form, and compared with Gaussian law. The kurtosis coefficient of z, K_z, and the correlation coefficient ρ between X_1 and X_2 are also indicated in the figure. For all cases, the measured values of $f(z)$ deviate from the Gaussian curve and K_z values differ from 3. The measured $f(z)$ values of SEST and BOMEX have very distinctive non-Gaussian forms.

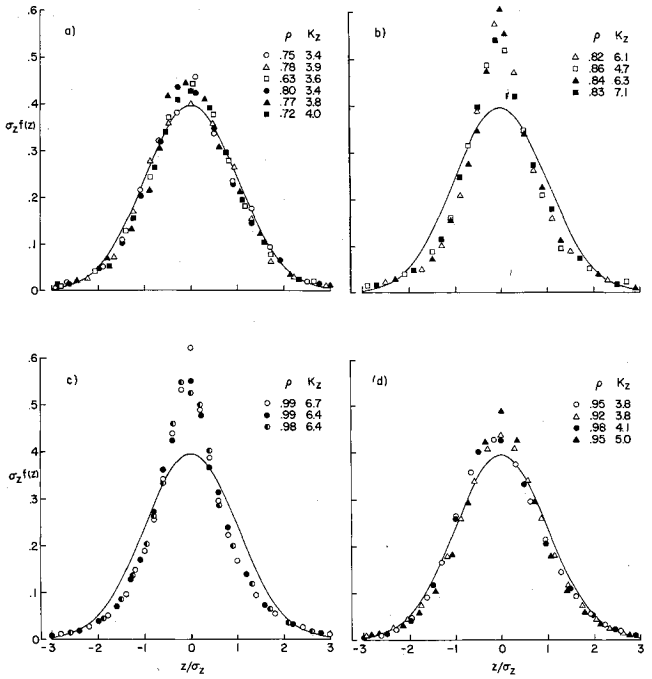

Fig. 2 Normalized probability density functions of Z compared with Gaussian law, where $Z = X(t + \tau) - X(t)$. All notes and symbols are the same as for Fig. 1.

For the cases of HICAT, greater deviations of $f(z)$ and K_z from Gaussian law might be expected if the ρ values were closer to 1, since kurtosis was found to be a smoothly decreasing function of τ when τ is not large.[7] Unfortunately, 0.8 is the highest ρ value available for observation because of the high-flying speed and low-sampling rate used during data acquisition. It is worthy of mentioning again that a ρ value close to 1 is one of the important conditions for arriving at Rice's simple equation. As for the cases of WITT, which have inherently very small turbulence Reynolds numbers, while the first-order distributions exhibit almost perfect Gaussian form the departure from Gaussian law for the second-order distributions is very apparent. The substantial departure indicates that $f(x_1, x_2)$ is strongly non-Gaussian, although the first-order distributions of $X(t)$ appear to be fairly Gaussian.

Conclusions

Joint normality of the second-order probability density is required to insure a successful application of Rice's exceedance statistics to atmospheric turbulence. The experimental results show that, in spite of Gaussian appearance for the first-order densities, the second-order densities invariably turn out to be strongly non-Gaussian. The kurtosis coefficients also depart greatly from 3, the Gaussian value. Thus, even stationary atmospheric turbulence cannot be considered a Gaussian process. And consequently, the application of Rice's equation should be approached with caution.

References

[1] Rice, S. O., "Mathematical Analysis of Random Noise," *Bell System Technical Journal*, Vol. 23, No. 3, July 1944, pp. 282–332, and Vol. 24, No. 1, Jan. 1945, pp. 46–156.

[2] Press, H. and Mazelsky, B., "A Study of the Application of Power-Spectral Methods of Generalized Harmonic Analysis to Gust Loads on Airplanes," Rept. 1172, 1954, NACA.

[3] Press, H., "Atmospheric Turbulence Environment With Special References to Continuous Turbulence," Rept. 115, AGARD, NATO, Paris, 1957.

[4] Rhyne, R. H. and Steiner, R., "Power Spectral Measurement of Atmospheric Turbulence in Severe Storms and Cumulus Clouds," TN D-2469, 1964, NASA.

[5] Crooks, W. M. et al., "Project HICAT-High Altitude Clear Air Turbulence Measurement and Meteorological Correlations," AFFDL-TR-68-127, Vol. I, 1968, Air Force Flight Dynamics Lab., Wright-Patterson Air Force Base, Ohio.

[6] Papoulis, A., *Probability, Random Variables, and Stochastic Processes*, McGraw-Hill, New York, 1965, Chap. 14.

[7] Van Atta, C. W. and Chen, W. Y., "Structure Functions of Turbulence in the Atmospheric Boundary Layer Over the Ocean," *Journal of Fluid Mechanics*, Vol. 44, 1970, pp. 145–159.

[8] Van Atta, C. W. and Chen, W. Y., "Measurements of Spectral Energy Transfer in Grid Turbulence," *Journal of Fluid Mechanics*, Vol. 38, 1969, pp. 743–763.

Improving Diffuser Performance by Artificial Means

V. Kr. Sháran*
The Royal Institute of Technology, Stockholm, Sweden

Introduction

ALTHOUGH a great deal of data on flow in diverging passages has been amassed in the past 115 yr, very little of it has been systematic. An effort was made to review the greater bulk of important diffuser performance results and a detailed investigation was started to understand the flow phenomena in parallel pipe for naturally developing flow and flow with fixed transition, and flow phenomena in conical diffusers. The ultimate aim was to separate out the effects of velocity profile and turbulence intensity on the performance of conical diffusers. Finally it was hoped to correlate diffuser performance with a combination of velocity profile and turbulence structure parameters. The earlier tendency of correlating diffuser performance with velocity profile parameters alone seems to be invalidated by the present results on static pressure rise coefficient.

Apparatus and Tests

Details of the experimental arrangement will be published later. Here only the salient features of the rig design are pointed out very briefly. The closed-circuit experimental rig is run by a 30 h.p. induction motor. The velocity range is 50–300 fps corresponding to Reynolds numbers of 1×10^5 to 4×10^5 (based on duct diameter), respectively. A parallel pipe, which is 150 duct diameters long, is joined to a diffuser, which is connected to the motor through a flexible pipe of 9 in. internal diameter.

A 16:1 area ratio contraction preceding the pipe gives a very flat, low-turbulence, uniform exit profile. The parallel pipe consists of 50 pipe sections each having an internal diameter of 4.06 ± 0.01 in. and length of 1 ft. There are static pressure taps of 0.06 in. diam and 4-in. pitch along three diametric planes at 120° to each other. The diffusers also have similar pressure taps. A heat exchanger is installed in the return circuit between the motor and the breather to keep the temperature of the rig constant, which otherwise tended to rise.

The test diffusers chosen, namely 5° and 15°, represent typically good and bad diffusers. The diffusers were made in four sections to enable the area ratios of 1.5, 2.5, 3.5, and 5.0 to be obtained. The test diffusers at the downstream end were followed by a 3-ft

Received January 31, 1972; revision received March 7, 1972. Acknowledgements are due to J. L. Livesey and J. Weir of the Mechanical Engineering Department of the University of Salford, England, where the above work was conducted.

Index category: Nozzles and Channel Flow.

* Research Fellow, Department of Aeronautics.